COBEM 2025
28TH INTERNATIONAL CONGRESS OF MECHANICAL ENGINEERING

ABCM
Brazilian Society of Mechanical Sciences and Engineering
28th ABCM International Congress of Mechanical Engineering
November 09-14, 2025, Curitiba-PR, Brazil

COB-2025-0682
INFLUENCE OF DAMS ON THE FLOW PATTERN IN A CONTINUOUS CASTING TUNDISH

Andreza Thomaz Quaresma
Ana Clara Santos Mauri
Renato do Nascimento Siqueira
João Paulo Barbosa
Federal Institute of Science and Technology of Espírito Santo – Campus São Mateus
andrezathomaz11@gmail.com
mauri09clara@gmail.com
renatons@ifes.edu.br
jpbarbosa@ifes.edu.br

Abstract. *The increasing demand for clean, high-quality steel makes the tundish stage in continuous casting a critical step in the manufacturing process. It is at this point that non-metallic inclusions are removed by flotation and absorbed by the slag layer at the surface. To enhance process efficiency and ensure product quality, flow-modifying devices such as weirs, dams, and turbulence inhibitors are incorporated into the tundish design. These elements optimize the flow of liquid steel and promote impurity separation. Dams, in particular, divide the tundish into two compartments and promote an upward redirection of the flow, increasing contact between inclusions and the slag. They also reduce fluid velocities compared to the inlet region, limiting the extent of the turbulent zone and bringing the flow regime closer to plug flow conditions. This study presents numerical simulations performed using the CFD software ANSYS Fluent R1 2025, considering different dam configurations with varying heights and positions. The objective is to identify flow patterns that facilitate inclusion removal and determine the most efficient geometric configuration. Evaluation criteria include residence time distribution (RTD) curves, hydraulic efficiency, and mixing indices. The results show that the presence of dams significantly changes the internal flow structure, promoting more favorable conditions for inclusion removal. An optimal dam height was identified: very low dams fail to produce meaningful improvements, while moderately high dams are more effective. However, excessively tall dams may compromise performance. Furthermore, when dams are placed too close to the outlet region, their positive effect is reduced due to limited flow redistribution. These findings support improvements in tundish design and contribute to the development of more efficient steel refining processes.*

Keywords: *dams, tundish, residence time distribution, computational fluids dynamics*

1. INTRODUCTION

Tundishes are intermediate reservoirs between the ladle and the molds in the continuous casting process, with the purpose of retaining the molten steel for a sufficient time and distributing it uniformly among the molds. With the increasing demand for clean and high-quality steels, the need to improve so-called tundish metallurgy has emerged. According to Mazumdar and Guthrie (1999), steel began to be subjected to stricter cleanliness and chemical composition requirements, transforming the tundish from a simple transfer channel into an active vessel for liquid steel refining, making it responsible for the removal of non-metallic inclusions. The presence of such inclusions in the final product significantly compromises its properties, making their removal essential to the refining process (Sahai, 2016).

The tundish can exhibit four flow zones: plug flow, complete mixing, short-circuiting, and dead volume. In plug flow, particles move in parallel and at a constant velocity. In complete mixing, fluid properties remain homogeneous at all locations and times. Short-circuiting refers to the preferential paths followed by fluid particles. Dead volume refers to regions where no property exchange occurs with the rest of the system, thus reducing the effective volume. According to de Almeida (1997), to ensure optimal hydrodynamic characteristics, it is desirable to maximize the fraction of plug flow, minimize short-circuiting, and reduce the dead volume fraction.

To achieve these hydrodynamic characteristics, and to facilitate the removal of non-metallic inclusions, flow-modifying devices are implemented within the tundish. To enhance the efficiency of this process, Sheng and Chen (2021) highlight the importance of these devices, which control flow patterns, increase the residence time of the fluid, and promote the separation of inclusions by flotation, directly contributing to higher steel quality. Among these devices, dams play a decisive role, as they can reduce dead zones and short-circuiting while favoring the flotation of inclusions (Kumar *et al.*, 2008). Furthermore, the efficiency of this effect strongly depends on the height and positioning of the dams, parameters that may significantly enhance or impair hydrodynamic performance (Jha *et al.*, 2008).

This article aims to analyze the effect of dam insertion on flow patterns in tundishes and their influence on hydrodynamic behavior, considering different height and positioning configurations. To this end, velocity fields are evaluated—an essential tool for identifying dead zones, preferential flow paths, and recirculation regions, along with residence time distribution (RTD) curves, from which information regarding hydraulic efficiency and mixing indices is extracted. Based on these analyses, dam configurations are identified that promote, through flow control, favorable conditions and an essential step, for the removal of non-metallic inclusions within the tundish.

2. CFD MODEL

2.1 Model Description

The simulations were performed using the commercial software ANSYS Fluent R1 2025, employing a three-dimensional model based on the Reynolds-Averaged Navier-Stokes (RANS) equations, with the Realizable $k-\epsilon$ turbulence model. The Realizable $k-\epsilon$ turbulence model was adopted as it presents better performance in predicting recirculations and separation zones, phenomena characteristic of tundish hydrodynamics, while maintaining low computational cost and wide reliability in fully turbulent flows. A water-based model was adopted to represent the flow phenomena in a single-strand tundish, allowing direct comparison with data from the literature, which commonly uses cold modeling to evaluate the hydraulic performance of tundishes. The top slag was not considered in the simulation, nor were the inclusions present in the molten steel included in the model. This simplification is justified since the main objective of this study is to analyze the velocity fields and flow patterns that favor the removal of inclusions. Therefore, the evaluation focuses on the hydraulic efficiency of the system, considering that well-distributed flows with reduced short-circuit zones are essential to optimize inclusion removal in actual metallurgical operations.

2.1.1 Fluid Flow

Equations 1 and 2 are used to describe the continuous phase of the model.
Continuity:

$$\frac{\partial \overline{U_i}}{\partial x_i} = 0 \tag{1}$$

where $\overline{U_i}$ are the mean velocity component and vector, respectively.
Momentum:

$$\frac{\partial \overline{U_i}}{\partial t} + \overline{U_j}\frac{\partial \overline{U_i}}{\partial x_j} = -\frac{1}{\rho}\frac{\partial}{\partial x_i}\left(\overline{P} + \frac{2}{3}\rho k\right) + \frac{\partial}{\partial x_j}\left[(\nu + \nu_t)\left(\frac{\partial \overline{U_i}}{\partial x_j} + \frac{\partial \overline{U_j}}{\partial x_i}\right)\right] \tag{2}$$

where $\overline{U_i}$, $\overline{P}$, ρ, ν, ν_t, and k are the mean velocity component, mean pressure, fluid density, kinematic viscosity, turbulent viscosity, and turbulent kinetic energy, respectively. The transport solution for turbulent kinetic energy is expressed by Eq. 3:

$$\frac{\partial k}{\partial t} + U_j\frac{\partial k}{\partial x_j} = \frac{\partial}{\partial x_j}\left[\left(\nu + \frac{\nu_t}{\sigma_k}\right)\frac{\partial k}{\partial x_j}\right] + P - \varepsilon \tag{3}$$

The transport equation for the dissipation rate of turbulent energy is given by Eq. 4:

$$\frac{\partial \varepsilon}{\partial t} + U_j\frac{\partial \varepsilon}{\partial x_j} = \frac{\partial}{\partial x_j}\left[\left(\nu + \frac{\nu_t}{\sigma_\varepsilon}\right)\frac{\partial \varepsilon}{\partial x_j}\right] + C_1\frac{\varepsilon}{k}P - C_2\frac{\varepsilon^2}{k} \tag{4}$$

where k represents the turbulent kinetic energy; ε is the turbulent energy dissipation rate; P indicates the production of turbulent kinetic energy; σ_k and σ_ε are the turbulent Prandtl numbers for k and ε, with values of 1.0 and 1.3, respectively; C_1 and C_2 are empirical constants equal to 1.44 and 1.92, respectively.

The kinematic viscosity ν_t used in Eqs. 2, 3 and 4 is defined by (Eq. 5):

$$\nu_t = C_\mu\frac{k^2}{\varepsilon} \tag{5}$$

where C_μ is an empirical, dimensionless constant that relates the turbulent viscosity to the turbulent kinetic energy and its dissipation rate.

2.1.2 Analysis of RTD Curve

Hydraulic efficiency and mixing indicators will be used to evaluate the flow patterns in the distributor. Teixeira and Siqueira (2008) investigated several indicators and identified those most suitable for representing the physical phenomena of short-circuiting and mixing. According to the authors, the initial passage time (t_i) and the time required for 10% of the tracer mass to reach the destination (t_{10}) are the best indicators of short-circuiting. For mixing characterization, the dispersion index (σ^2) and the Morril index (Mo) stand out. The σ^2 index is given by the ratio between the variance of the passage curve and the mean detention time. The Mo index corresponds to the ratio between the passage times at the outlet of the unit for 90% and 10% of the tracer mass injected at the inlet.

2.1.3 Tracer Dispersion

To calculate the concentration of the additive tracer, the transport of a passive scalar is simulated by solving a filtered advection-diffusion (Eq. 6). This equation is solved at each time step, considering that the fluid field has already been previously calculated.

$$\frac{\partial \overline{C}}{\partial t} + U_j \frac{\partial \overline{C}}{\partial x_j} = \frac{\partial}{\partial x_j}\left[\left(D_m + \frac{\nu_t}{S_{ct}}\right)\frac{\partial \overline{C}}{\partial x_j}\right] \tag{6}$$

where $\overline{C}$ is the mean concentration, D_m is the molecular diffusion coefficient and S_{ct} is the turbulent Schmidt number, considered as $S_{ct} = 0.7$ in this study.

The velocity field U_j is obtained from a steady-state simulation and remains constant during the calculation of the passive scalar.

2.2 Geometry and Boundary Conditions

The geometry used (Fig. 1) was adapted from Maurya and Jha (2014) and represents a simplified version of a single-wire tundish with a maximum capacity of $4.77\,\mathrm{m}^3$. The inlet and outlet have diameters of $0.09\,\mathrm{m}$ and are positioned $0.4\,\mathrm{m}$ from the left wall on the upper surface and $0.4\,\mathrm{m}$ from the right wall on the lower surface, respectively. The front and side walls have a $14°$ inclination. The tundish includes a weir with a width of $0.05\,\mathrm{m}$ positioned along the flow path. The other dimensions are shown in Fig. 1 (b) and (c).

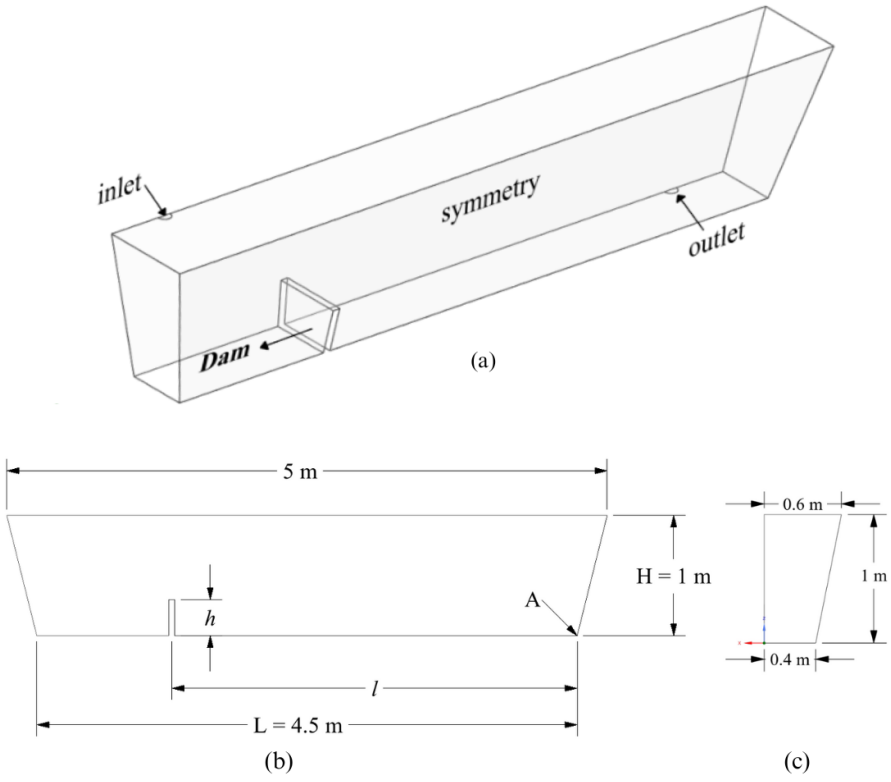

Figure 1. (a) Geometry of the single strand tundish (b) & (c) Side views of the tundish

Figure 1 (b) the reference parameters used to define the dam heights and positions. The length l is measured from point A to the center of the dam. Four different dimensionless heights (h_1, h_2, h_3, h_4) and four different dimensionless positions (l_1, l_2, l_3, l_4) were selected. The heights h_i are defined as the ratio of the dam height (h_i) to the tundish height H, while the positions l_i represent the ratio between the distance from the center of the dam to point A and the total tundish width L. Table 1 summarizes the different dam configurations analyzed.

Table 1. Description of variations in position and height of the dam in the tundish.

h_1	h_2	h_3	h_4	l_1	l_2	l_3	l_4
0.30	0.40	0.50	0.60	0.90	0.75	0.60	0.45

The initial simulations were conducted by fixing the position l_2 and varying the overall height. Based on the analysis of the optimal configuration, three further cases were evaluated by modifying the remaining three positions.
No-slip conditions were applied to all walls except the top surface, which was set as a free-slip boundary. A symmetry condition was applied to simulate only half of the domain, reducing computational cost. The inlet velocity was fixed at 1.4 m/s and atmospheric pressure was defined as the outlet condition.

2.2.1 Solution Procedure

The discretized equations were solved using the Semi-Implicit Method for Pressure-Linked Equations (SIMPLE) algorithm for the steady-state simulation and the Coupled algorithm for the transient simulation.

To solve the passive scalar equation, a zero mass flux boundary condition was applied to the walls and to the top surface of the domain. After the steady-state flow was established, the mass fraction of the tracer at the inlet was set to 1 for the first 0.2 seconds of the simulation and then reduced to zero for 0.2 s, representing a pulse injection. The tracer concentration at the outlet was monitored over time, allowing the residence time distribution (RTD) curves to be obtained through numerical calculation.

Considering the inlet velocity of 1.4 , m/s , the inlet diameter of 0.09 m, and the physical properties of water at room temperature ($\rho = 998.2\,\text{kg/m}^3$, $\mu = 1.002 \times 10^{-3}$ Pa·s), the Reynolds number was estimated as approximately 1.26×10^5, which characterizes the flow as fully turbulent. All simulated conditions maintained Reynolds numbers of the same order of magnitude, ensuring a turbulent regime throughout the tundish domain.

2.2.2 Numerical Modelling Details

An overview of the fluid properties and solution methods are listed on Tab. 2

Table 2. Numerical Simulation Parameters

Category / Parameter Detail			**Value/Method**
Material (Water)	Density (ρ)		998.2 kg/m^3
	Molecular viscosity (μ)		1.002×10^{-3} Pa s
Solution Methods	Time Step Size (transient)		0.05 s
	Number of Time Steps (transient)		48000
	Pressure-Velocity Coupling		SIMPLE (Steady) Coupled (Transient)
	Spatial Discretization	Gradient	Least Squares Cell Based
		Pressure	Second Order
		Momentum	Second Order Upwind
		Turbulence Model	k-ϵ Realizable
		Turbulent kinetic energy (k)	Second Order Upwind
		Turbulent dissipation rate (ϵ)	Second Order Upwind
	Transient Formulation		Second Order Implicit
	Convergence Criterion		10^{-4}
Tracer Injection (RTD Curve)			IF (flow_time<0.2[s],1,0)

3. VERIFICATION AND VALIDATION OF CFD MODEL

3.1 Sensitivity Study of Mesh

To ensure the independence and accuracy of the results in a CFD analysis, it is essential to use a refined and high-quality mesh. As shown in Fig. 2, a mesh independence study was conducted to verify the adequacy of the discretization adopted, using prismatic element meshes.

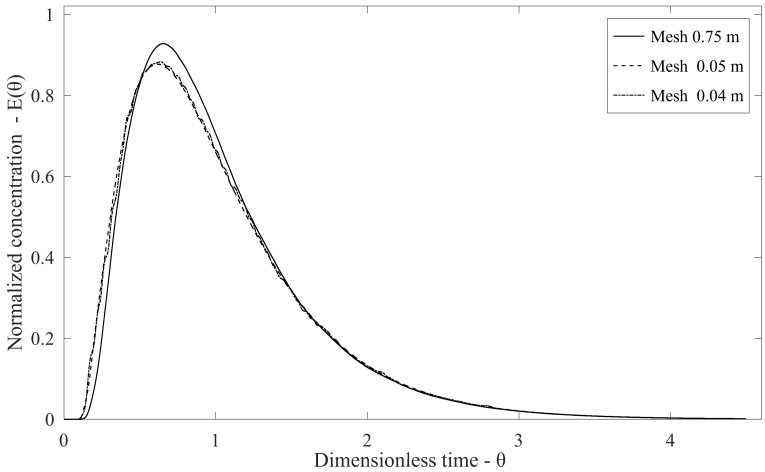

Figure 2. Comparison of calculated E-curves with different CFD mesh sizes.

The comparison between the meshes revealed significant variations in some indicators, while others showed only slight differences. The meshes with sizes of 0.05 m and 0.04 m exhibited differences of 3% and 11% in the Mo and σ^2 indicators, respectively. However, despite offering greater accuracy, the 0.04 m mesh comes with a higher computational cost. In contrast, the 0.075 m mesh, although computationally more efficient, showed more pronounced differences in all indicators compared to the 0.05 m mesh, such as the 20% discrepancy in the Mo indicator. To strike a balance between computational cost and result accuracy, the study adopted the mesh with 107,492 elements and a reference size of 0.05 m.

3.2 Validation of CFD Modelling

The CFD model was validated by comparison with experimental data from a water physical model, as reported by Chen *et al.* (2014). The Residence Time Distribution (RTD) curves obtained from the CFD simulations are presented in Figure 3, together with the experimental results from the water physical model. The detailed input data used for the CFD simulations, including hydrodynamic parameters and material properties, are available in Chen *et al.* (2014). The tracer injection in the simulations was performed as a pulse injection, with a constant injection of one unit from time 0 to approximately 2 s; for times greater than 2 s, the injection rate was set to zero.

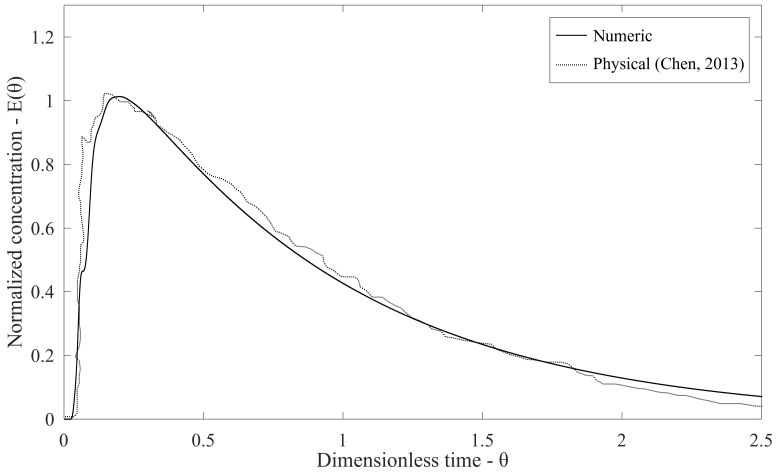

Figure 3. RTD curve obtained from the CFD simulation.

There is good agreement between the experimental data and the numerical results obtained in this study. The peak values of the curves show good consistency, and the slope of the curves after the peak also exhibits a coherent behavior between the experimental and simulated results. The CFD simulation results showed good agreement with the experimental data, indicating that the comparison between the CFD simulation and the experiment is satisfactory for model validation.

4. RESULTS AND DISCUSSION

4.1 Influence of Dam Height

The steady-state simulation provides the velocity fields for the different dam height configurations, allowing the visualization of recirculations, stagnation regions, and flow stability zones. Fig. 4 presents the velocity fields corresponding to the heights h_1, h_2, h_3 and h_4, while keeping the position l_2 fixed.

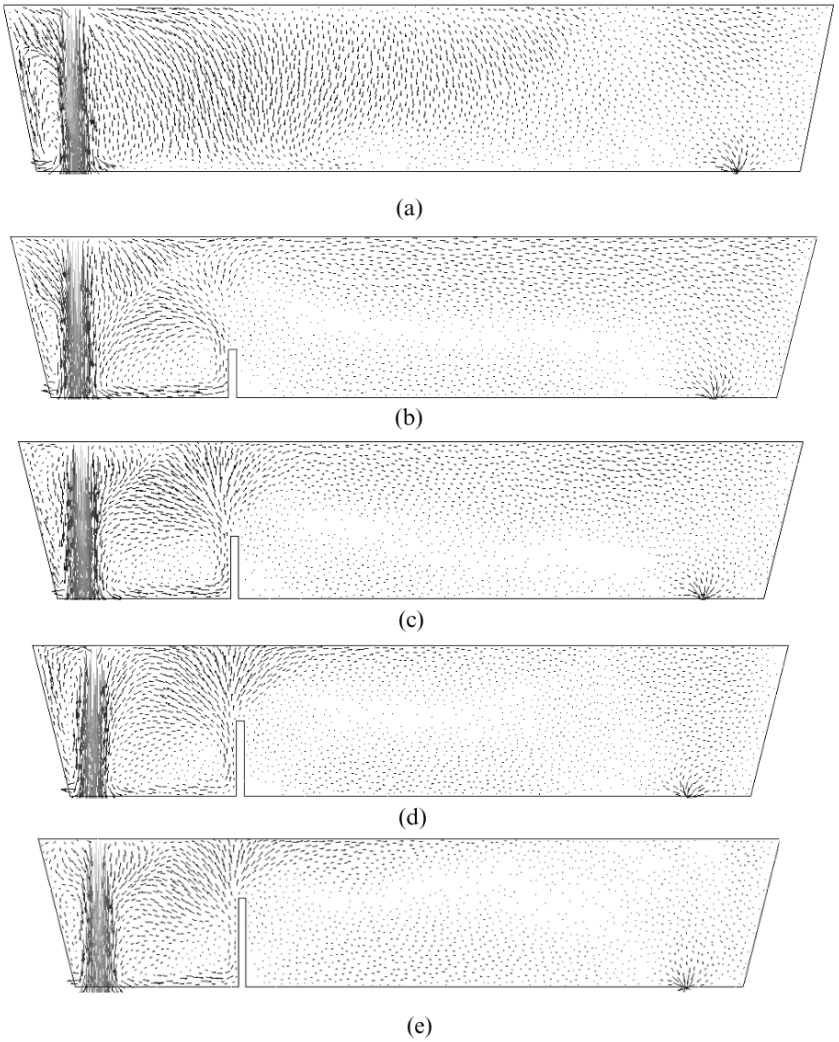

Figure 4. Velocity fields for (a) Bare Tundish (b) h_1 (c) h_2 (d) h_3 (d) h_4

In Figure 4 (a), it is noted that the distributor without any dam shows a flow with large high-velocity regions, allowing the fluid to pass through the unit in a shorter time, resulting in a reduced residence time. Figure 4 (b) demonstrates that, with the insertion of the dam at height h_1, the flow is redirected, and stagnation zones are formed immediately downstream of the dam, which contributes to reducing the velocity in the downstream regions. In Figure 4 (c), the formation of recirculation zones upstream of the dam is observed, while stagnation zones persist downstream, providing a more uniform velocity distribution. Figure 4 (d) indicates that, for the dam height h_3, the flow is more strongly retained in the inlet region, and downstream of the dam there is a significant reduction in velocity, with the flow being predominantly directed towards the upper region of the domain. Finally, in Figure 4 (e), it is verified that for the highest dam height, there is a considerable increase in the stagnation region downstream of the barrier; however, the flow is not as efficiently directed upwards as in the previous configuration.

Figure 5 displays the RTD curves for the different dam height configurations and the results of the hydraulic efficiency

indicators obtained through the RTD curve are shown in Tab. 3.

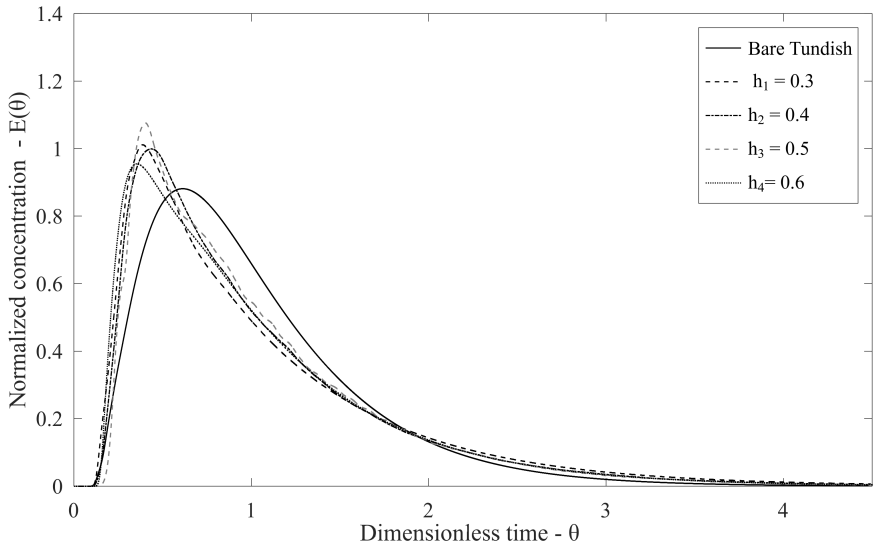

Figure 5. Residence Time Distribution (RTD) curves for different dam height configurations.

Table 3. Mixing and hydraulic efficiency indicators obtained from the RTD curve for height variation.

Configuration	**Residence Time Indicators**			
	t_i	t_{10}	Mo	σ^2
Bare tundish	0.10	0.36	5.05	0.38
h_1	0.11	0.32	6.42	0.53
h_2	0.12	0.34	5.76	0.49
h_3	0.16	0.36	5.42	0.46
h_4	0.13	0.32	6.20	0.50

The results summarized in Table 3 indicate that the bare tundish presents the lowest t_i, confirming the presence of more significant short-circuiting compared to the other configurations. The h_1 and h_2 cases present similar values for the hydraulic indicators, although h_2 has slightly lower M_0 and σ^2, suggesting a more homogeneous and less dispersed flow. The h_3 case shows the highest t_i value, indicating a more effective reduction of short-circuiting. Although its M_0 and σ^2 values do not differ significantly from other cases, the greater initial fluid retention and more controlled flow behavior point to superior hydraulic efficiency. The case with height h_4 presents a lower t_i value compared to h_3, indicating a higher degree of short-circuiting. This demonstrates that there is a limit beyond which increasing the dam height no longer yields significant improvements in hydraulic performance. Therefore, height h_3 is considered the most effective, as it reduces short-circuiting risk, improves flow control, increases fluid residence time, and provides favorable conditions for the removal of non-metallic inclusions in the tundish.

4.2 Influence of Dam Position

With the choice of h_3 as the best height, the variation of the positions were made and the velocity fields are shown in Fig. 6. The velocity fields presented in Fig. 6 (b) show that the dam placed at position l_1 has a limited effect on modifying the flow pattern. This is due to its proximity to the inlet jet region, where turbulence levels are extremely high. As a result, the dam does not have enough distance to dissipate the jet's kinetic energy effectively, leading to the persistence of high-velocity regions immediately downstream. In contrast, Fig. 6 (c), corresponding to position l_2, demonstrates significantly better performance. The increased distance from the inlet allows the dam to act more effectively, containing the highly turbulent zone and reducing the velocity field in the downstream region. This configuration promotes a more uniform flow distribution and enhances flow stability within the tundish. Figs. 6 (d) and (e), representing positions l_3 and l_4, reveal that placing the dam too far from the inlet diminishes its effectiveness. In these cases, the inlet jet's energy dissipates substantially before interacting with the dam. Consequently, the structure fails to significantly influence the flow pattern, limiting its ability to reduce velocity and redirect the flow. This condition allows part of the fluid to move directly toward the outlet without proper redirection, increasing the risk of short-circuiting and compromising the tundish's hydraulic efficiency.

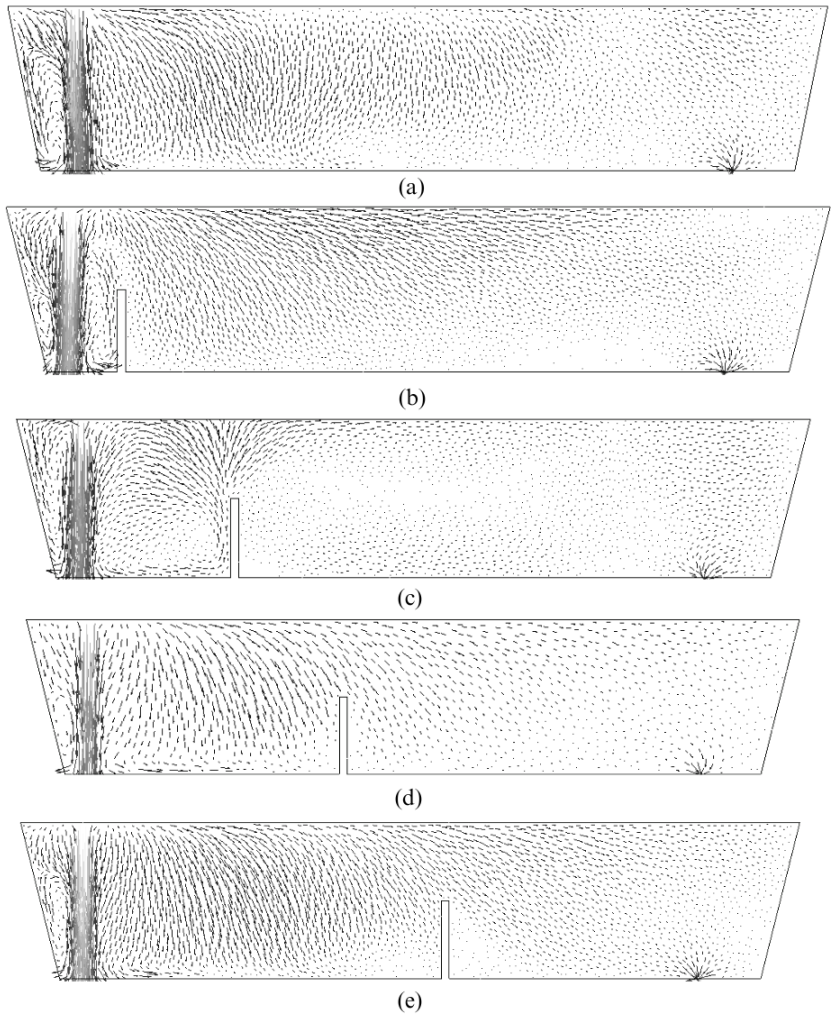

Figure 6. Velocity fields for (a) Bare Tundish (b) h_1 (c) h_2 (d) h_3 (e)h_4

The (RTD) curves were also obtained for the position variation and can be observed in Fig. 7:

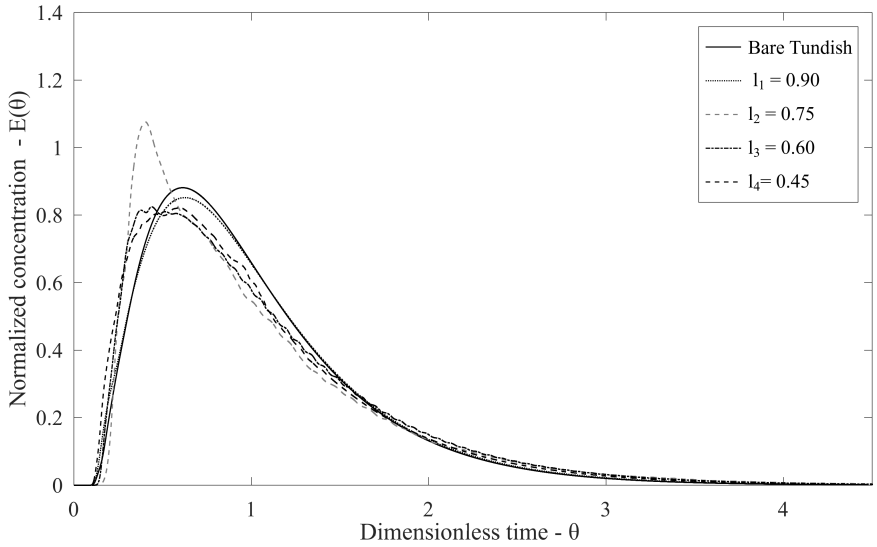

Figure 7. Residence Time Distribution (RTD) curves for different dam position configurations.

The hydraulic efficiency and mixing indicators extracted from the curve (Fig. 7) are presented in Tab. 4:

Table 4. Mixing and hydraulic efficiency indicators obtained from the RTD curve for position variation.

Configuration	**Residence Time Indicators**			
	t_i	t_{10}	Mo	σ^2
Bare tundish	0.10	0.36	5.05	0.38
l_1	0.11	0.39	4.74	0.37
l_2	0.16	0.36	5.42	0.46
l_3	0.11	0.39	4.79	0.37
l_4	0.10	0.34	5.62	0.44

The Table 4 shows that the bare tundish, as well as the configurations with dams positioned at l_1, l_3, and l_4, present very similar t_i values, indicating a comparable behavior regarding the degree of short-circuiting. It is observed that the l_1 and l_3 cases have very similar indicators, both associated with a higher degree of short-circuiting and lower mixing efficiency. This behavior reinforces that there is an optimal position for the installation of the dam, which should be neither too close to the inlet nor too far from it. The configuration with the dam at position l_2 presents the highest t_i value, which indicates greater mitigation of short-circuiting. Furthermore, this case shows the second-highest M_O and the highest σ^2, indicating an improvement in hydraulic efficiency accompanied by a greater intensity of mixing. On the other hand, the l_4 position shows low t_i and t_{10} values, characterizing a higher degree of short-circuiting. This confirms that the greater the distance between the inlet and the dam, the lower the efficiency of the device in promoting proper flow distribution and homogenization. Seeking better overall efficiency among the indicators analyzed, the l_2 position stands out, as it reduces short-circuiting, improves hydraulic efficiency, and provides a more homogeneous mixture compared to the other configurations.
Considering the overall efficiency among the analyzed indicators, the l_2 position stands out, as it reduces short-circuiting, improves hydraulic efficiency, and provides a more homogeneous mixture compared to the other configurations. The best geometric configuration of the dam, among the tested cases and obtained results, based on velocity contours, residence time distribution (RTD) curves, and the performance of hydraulic efficiency and mixing indicators, was the one with height h_3 and position l_2. Dead zones were identified through the analysis of velocity fields and mixing criteria, corresponding to regions of low velocity and little variation in tracer concentration over time. These areas exhibit longer residence times and lower mixing efficiency, reflected in the low values of the Morril index (Mo) and dispersion index (σ^2), allowing a direct correlation between hydraulic performance and the flow distribution within the tundish.

5. CONCLUSIONS

The numerical analysis carried out to determine the optimal geometric configuration of the dam within the tundish, based on velocity contours and parameters obtained from the residence time distribution (RTD) curve, indicated that the configuration with height h_3 and position l_2 exhibited the best performance in terms of hydraulic efficiency and inclusion removal. The results demonstrated the existence of an optimal dam height, where excessively high values tend to promote hydraulic short-circuiting, while overly low heights lead to the formation of stagnant flow regions. Similarly, positioning the dam too far from the inlet negatively affects the flow distribution and residence time characteristics. It is important to highlight that the analysis was limited to the set of cases evaluated, and more efficient dam geometries may exist. Furthermore, the results suggest that, in order to maximize the metallurgical refining efficiency in the tundish, the dam should be combined with other flow control and modifying devices.

6. ACKNOWLEDGEMENTS

This work was carried out with support from the Espírito Santo Research and Innovation Support Foundation (FAPES - Fundação de Amparo à Pesquisa e Inovação do Espírito Santo) – T.O. 1052/2022. The authors also thank FAPES for the grant funding that enabled this study to be conducted.

7. REFERENCES

Chen, D., Xie, X., Long, M., Zhang, M., Zhang, L. and Liao, Q., 2014. "Hydraulics and mathematics simulation on the weir and gas curtain in tundish of ultrathick slab continuous casting". *Metallurgical and Materials Transactions B*, Vol. 45, No. 2, pp. 392–398.

de Almeida, M.M.P., 1997. *Study of the effect of flow deflectors and of the effective length-to-width ratio on the hydraulic efficiency of sedimentation basins*. Master's thesis, Graduate Program in Sanitary and Environmental Engineering, Federal University of Espírito Santo, Vitória, Brazil.

Jha, P.K., Rao, P.S. and Dewan, A., 2008. "Effect of height and position of dams on inclusion removal in a six strand tundish". *ISIJ International*, Vol. 48, No. 2, pp. 154–163.

Kumar, A., Mazumdar, D. and Koria, S.C., 2008. "Modeling of fluid flow and residence time distribution in a four-strand tundish for enhancing inclusion removal". *ISIJ International*, Vol. 48, No. 1, pp. 38–47.

Maurya, A. and Jha, P., 2014. "Study of inclusion removal in a single strand tundish with varying dam height and position". In *Proceedings of the Conference Processing and Fabrication of Advanced Materials (PFAM 2014)*.

Mazumdar, D. and Guthrie, R.I.L., 1999. "The physical and mathematical modelling of continuous casting tundish systems". *ISIJ International*, Vol. 39, pp. 524–547.

Sahai, Y., 2016. "Tundish technology for casting clean steel: A review". *Metallurgical and Materials Transactions B*, Vol. 47, pp. 2095–2106.

Sheng, D.Y. and Chen, D., 2021. "Comparison of fluid flow and temperature distribution in a single-strand tundish with different flow control devices". *Metals*, Vol. 11, No. 5.

Teixeira, E.C. and Siqueira, R.d.N., 2008. "Performance assessment of hydraulic efficiency indexes". *Journal of Environmental Engineering*, Vol. 134, No. 10, pp. 851–859.

8. RESPONSIBILITY NOTICE

The authors are solely responsible for the printed material included in this paper.